Int J Adv Manuf Technol (2017) 93:1079–1094
DOI 10.1007/s00170-017-0445-4

ORIGINAL ARTICLE

Effective methods for fabricating trapezoidal shape microchannel of arbitrary dimensions on polymethyl methacrylate (PMMA) substrate by a CO_2 laser

SiJie Zhang[1] · **Yung C. Shin**[1]

Received: 9 February 2017 / Accepted: 21 April 2017 / Published online: 3 June 2017

Abstract The typical triangular-shaped microchannels fabricated by CO_2 laser-based microchanneling of polymethyl methacrylate yield low performance in heat sinks, chemical reactors, and other microfluidic devices. Trapezoidal and rectangular microchannels are more commonly used and desired. To fabricate high-quality trapezoidal microchannels using a CO_2 laser on polymethyl methacrylate substrates, a two-pass fabrication method is introduced using the offset ratio of 45% to yield a clean cross section. To determine the optimal process parameters to achieve trapezoidal microchannels of desired dimensions, the effects of process parameters were further investigated and groups of equations were derived based on nonlinear regression models. A microfluidic chip was fabricated to compare the performance of triangular and trapezoidal microchannels of the same cross sectional area. The results demonstrated the superior performance of the trapezoidal microchannel fabricated using two-pass fabrication. This indicates that the two-pass fabrication method is a viable rapid and economic solution for fabrication of high-quality microchannels on polymethyl methacrylate-based devices.

Keywords Trapezoidal channel · Microchannel machining · PMMA · CO_2 laser ablation

✉ Yung C. Shin
shin@purdue.edu

[1] School of Mechanical Engineering, Purdue University, West Lafayette, IN 47907, USA

1 Introduction

The last decade witnessed the significant progress made in the development of microfluidic devices for biomedical and biochemical applications. The microchannel is a basic element in these devices, which are used as a network to perform mixing, chemical reaction, particle detection, particle separation, and so on [1]. Those devices are usually fabricated on silicon and glass substrates, which are costly for disposable microfluidic devices. Polymethyl methacrylate (PMMA) is an important, low-cost alternative to silicon and glass. PMMA also has other advantages like reduced contamination effects and resistance to hydrolysis and chemical inertness in neutral aqueous solutions [2].

Several conventional microfabrication methods have been proposed for polymer-based microfluidic devices including hot embossing, injection molding, microthermoforming, casting [3], and micromilling [4]. However, these methods are either complex or of low efficiency. CO_2 laser direct-writing ablation provides a highly effective and low-cost way for micromachining. It also has the advantages of being flexible and environmental friendly compared with conventional methods [1].

Various groups have investigated fabricating microchannels on PMMA substrates using a CO_2 laser system in recent years. Klank et al. [5] first utilized a commercial CO_2 laser system to fabricate microchannels on PMMA substrates. Snakenborg et al. [6] presented an optimal cutting sequence for making a T-junction to minimize the deposited PMMA in the microchannel. Prakash et al. [7] developed a 2D model based on energy conservation regardless of heat transfer and melting effect for predicting the microchannel profile in single-pass and two-pass CO_2 laser microchanneling processes. A simultaneous thermogravimetric analysis/differential scanning calorimetry (TGA/DSC) test was performed in their work to obtain

the thermal properties of PMMA. Xiang et al. [8] presented a three-dimensional transient finite element model based on energy conservation and heat conduction theory for predicting the groove profile of the microchannel and the temperature distribution through the process. Romoli et al. [9] tried multiple-pass CO_2 laser microchanneling with spacing between each groove to fabricate cavities on PMMA. However, the cavities were of low flatness with periodical humps appearing at the bottom region. Also, it required too many passes, which would lower the process efficiency.

The problems associated with CO_2 laser micromachining on PMMA substrates have also been discussed. Formation of bulges at the rim of the microchannel is a big problem in laser-assisted fabrication techniques. This problem will cause the leak of the fluid samples because the region beside the bulges will not be fully sealed during the bonding process [9]. Adding an additional layer to the PMMA substrate before an ablation process was conceived as a method to eliminate the bulge. Chung et al. implemented an additional layer of PDMS, unexposed photoresist [10] and metal films with patterns [11], during the laser ablation process and successfully reduced the characteristic bulge on the rim of the microchannel. The metal films served as a physical shield to limit the microchannel width and to prevent resolidification and clogging in the microchannel junctions. Li et al. [12] presented an experimental and theoretical investigation into the formation and elimination of the bulges. They recorded the formation process of bulges using a stereo light microscope (SLM) system. They pointed out that the bulges are formed due to the extrusion of the softened polymer material by thermal stresses. They used a finite element model to establish a relationship between line energy and the height of bulge and also purposed a two-time cutting method to eliminate the bulges. Nayak et al. [13] investigated the effect of polymer molecular weight on CO_2 laser micromachining. They pointed out that the formation of the bulge is due to the lowering of polymer density and ejected and resolidified PMMA. It was found that when molecular weight is 96.7 kDa, no bulge is formed. When molecular weight is larger than 120 kDa, bulges start to form and PMMA with lower molecular weight tends to form bigger bulges under the same process parameters. It was also found that pore formation increased with an increase in molecular weight, which will cause an increase of surface roughness on the microchannel wall.

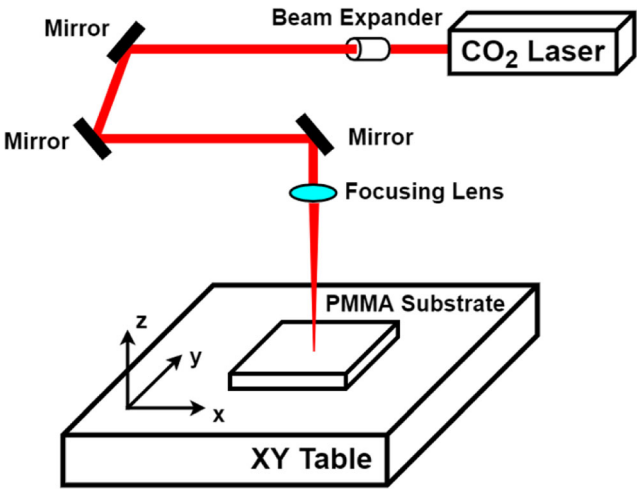

Fig. 1 Schematic diagram of a CO_2 laser micromachining system

Table 1 Description of Synrad 48-2 CO_2 Laser

Maximum output power	25 W
Mode quality	$M^2 < 1.2$
Ellipticity	<1.2
Beam diameter	3.5 mm
Beam divergence (full angle)	4 mrad
Wavelength	10.57–10.63 μm

Surface roughness of the channel wall is also a problem for CO_2 laser machining. Huang et al. [14] found that the surface roughness is due to the residues on the laser-cut edge caused by the bursting of the bubbles. They reduced the roughness by preheating the PMMA substrates to the temperature of 70–90 °C. Hong et al. [2] successfully utilized the method of fabricating microchannels on PMMA substrates using an unfocused beam to improve the surface roughness of the microchannel wall without further annealing operations.

Although many studies have been done on CO_2 laser microchanneling on PMMA, little attention was paid on the cross section shape fabricated using this method. The cross section shape has a large influence on the performance of a microchannel in terms of heat transfer and flow behavior. Multiple researchers have found that the trapezoidal microchannel is superior to the triangular cross section in microfluidic chemical reactors [15] and heat sinks [16]. However, due to the Gaussian beam distribution of the CO_2 laser, microchannels fabricated by CO_2 laser micromachining have a triangular cross section [7]. This triangular groove shape is problematic because it limits the flux that can pass through the microchannel and will result in bigger pressure drop compared to a trapezoidal or rectangular groove shape [16]. Several studies were conducted to solve this triangular groove shape problem using a femtosecond laser. The methods presented either involve complex optics and beam shaping [17] or require too many scanning passes [18], which will take a long process time. In addition, femtosecond lasers

Table 2 Thermal property of PMMA [7]

Glass transition temperature	105 °C
Melting temperature	165 °C
Thermal decomposition begins	230 °C
Fully vaporized	393 °C

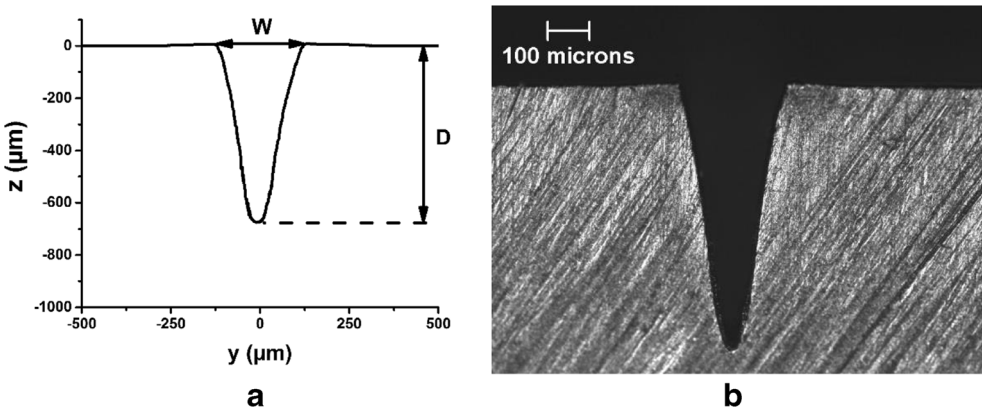

Fig. 2 Groove profile of the microchannel fabricated by one-pass scanning with $P = 6$ W E = 320 J/m measured by **a** 3D optical microscope and **b** optical microscope

are costly and less industrially ready. So far, no research was conducted on providing an economic solution to fabricate a higher-quality microchannel on PMMA.

This study presents a two-pass fabrication method to fabricate a trapezoidal grooved microchannel of high quality. The effect of the process parameters involved in this process, namely, the offset, power, and line energy, is first investigated. In order to obtain the process parameters for fabricating the microchannel of desired dimensions, regression models are first built to predict the key dimensional parameters of the microchannel fabricated by one-time pass. Based on this regression model and the optimized line energy relationship of two passes, a group of equations for finding the process parameters are developed. To compare the performance between the conventional triangular microchannel and the trapezoidal microchannel, a microchip with two parallel 3-mm-long microchannels was made. The microchannels were tested using a syringe pumping system. The result showed that for microchannels of the same cross sectional area, the trapezoidal microchannel has a lower pressure drop and has a better performance than the conventional triangular microchannel. Also, the experimental results confirm that two-pass CO_2 laser microchanneling is an economic and highly efficient way of producing high-quality microchannels.

2 Materials and experimental setup

Figure 1 schematically illustrates the experimental setup. A CO_2 laser system (Synrad 48-2) with a maximum output power of 25 W was used in continuous wave mode. The laser had an almost Gaussian TEM ($M^2 < 1.2$), and other specifications of the laser are shown in Table 1.

A lens with the focal length of 76.2 mm was used to limit the beam width to 250 μm. Previous studies [7] showed that an unfocused beam would yield a microchannel with a Gaussian cross section shape with a low aspect ratio. The focused beam was therefore used throughout the experiment to achieve the microchannel with minimal taper. The focused beam was scanned over the PMMA substrate perpendicularly by using an X-Y table driven by DC motors with a 25 nm resolution. The maximum scanning speed is 130 mm/s. The PMMA substrates were optically clear cast acrylic with the dimension of 100 mm × 40 mm × 5 mm. The thermal properties of the PMMA are reported in Table 2. The substrates were

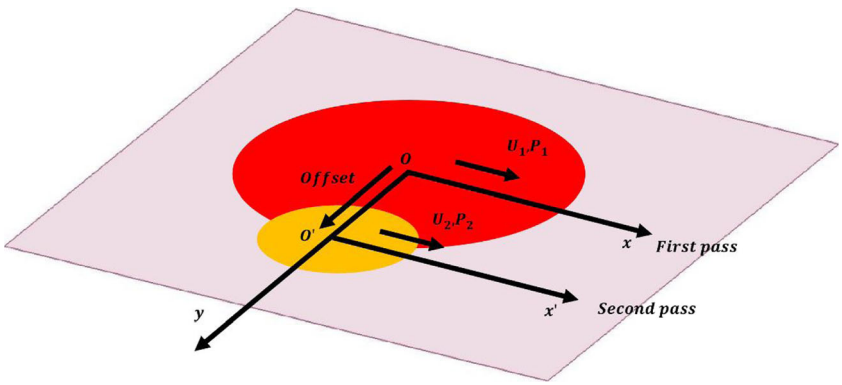

Fig. 3 Illustration of a two-pass fabrication method

attached to the X-Y table, and the microchannels were fabricated for 100 mm length on the x-axis, which was subsequently cut into substrates with dimension of 55 mm × 40 mm × 5 mm. The cross section of the microchannel was observed using an optical microscope.

In order to get quantitative results, a 3D optical profilometer (Bruker GTK) was used to measure the profiles of the microchannel. The 3D optical profiler measured the profile of the microchannel based on coherence scanning interferometry. The 3D optical profiler was operated in vertical scanning interferometry (VSI) mode, and an F-Operator was used to remove the modal tilt of the raw data.

The experiment for each set of process parameters was repeated at least twice to test the repeatability. Three cross section profiles of each microchannel made were chosen randomly along the x-axis to do the measurements, thus resulting in a total of six measurements per microchannel fabricated. The dimensional parameters are reported in terms of mean and 95% confidence limits.

3 Two-pass fabrication method

3.1 Process parameters

The microchannels fabricated by conventional single pass scanning have triangular grooves. As shown in Fig. 2, the width varies a lot with channel depth. This triangular groove will result in a larger pressure drop compared to a trapezoidal or rectangular microchannel [16]. This large variation with channel depth will also cause a huge difference in the flow and heat transfer behavior between the top and bottom portions of the microchannel. These triangular microchannels will therefore yield lower-performance microfluidic devices.

A two-pass fabrication method is introduced to fabricate the microchannel with a trapezoidal groove of higher quality. This method is illustrated in Fig. 3. A microchannel is fabricated by two passes of laser ablation where the second pass has an offset with respect to the first laser pass. O and O' are the centers of the first pass and the second pass, respectively. P_1 and P_2 are denoted as the laser power of the first and second passes, respectively. U_1 and U_2 denote the scanning speed of the first and second passes, respectively. The offset ratio is selected as a percentage of offset to the microchannel width fabricated by the first pass W_1 and is defined by Eq. 1.

$$\text{Offset ratio} = \frac{\text{Offset}}{W_1} \times 100\% \tag{1}$$

From previous research [9], it was found that the width and depth of the microchannel are approximately proportional to the inverse of the scanning speed, namely, $1/U$, while the actual width and depth will vary according to the laser power and scanning speed. Directly using scanning speed as an independent process parameter for experimental design and regression model development will be problematic due to the nonlinear effect. In order to avoid that, the line energy is introduced as a new independent variable, which can be defined by Eq. 2.

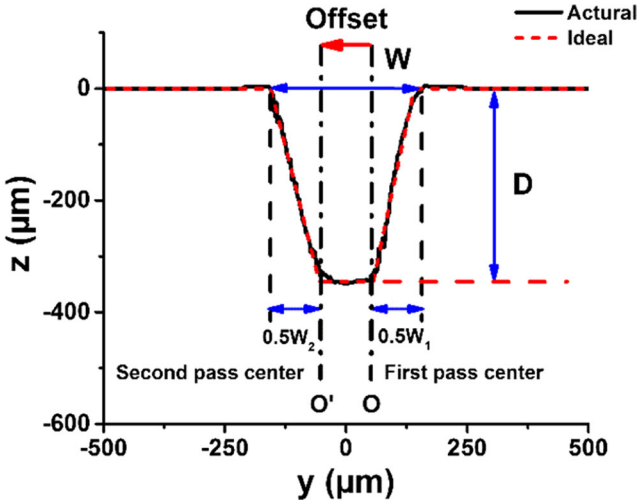

Fig. 4 Groove profile of a microchannel fabricated by two-pass scanning using $P_1 = P_2 = 4W$ $E_1 = 160$J/m $E_2 = 105.6$J/m, Offset ratio = 45% measured by a 3D optical microscope

$$E = \frac{P}{U} \tag{2}$$

where P is the laser power and U is the scanning speed.

3.2 Dimensional parameters

Figure 4 shows the groove profile of the microchannel fabricated by the two-pass fabrication method using laser power P_1 and P_2 of 4 W and scanning speed U_1 of 25 mm/s and U_2 of

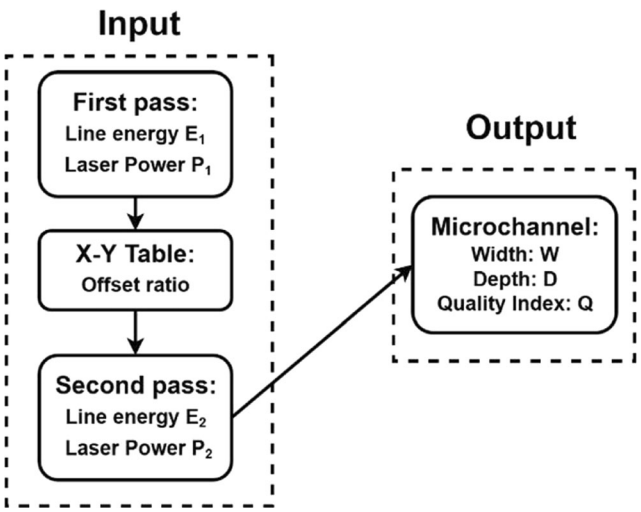

Fig. 5 Input and output parameters of a two-pass fabrication method

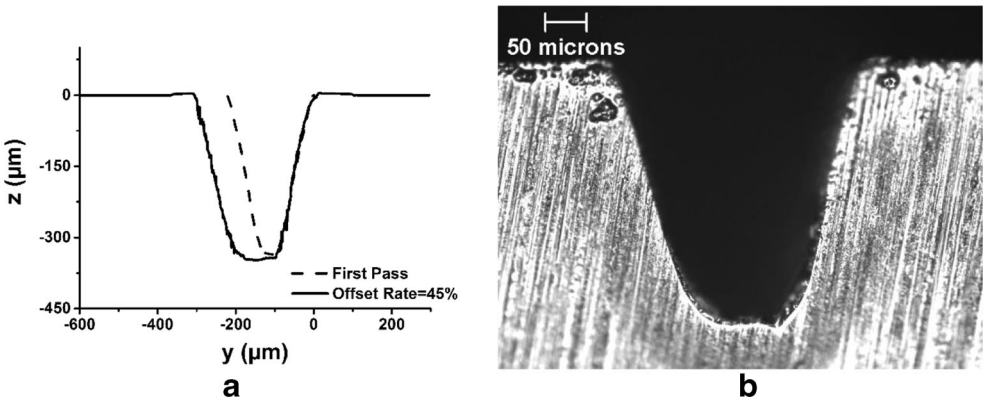

Fig. 6 Groove profile of a microchannel fabricated by two-pass scanning using $P_1 = P_2 = 4$W $E_1 = 160$J/m $E_2 = 105.6$J/m, Offset ratio = 45% measured by **a** 3D optical microscope and **b** optical microscope

37.88 mm/s with the offset of 45% W_1. The solid line is the actual groove shape, and the dashed line is the ideal groove shape. Several key parameters can be used to describe the microchannel shown in Fig. 4. W is the width of the microchannel, which can be estimated by Eq. 2.

$$W = 0.5W_1 + \text{Offset} + 0.5W_2 \tag{3}$$

where W_1 and W_2 are the microchannel widths fabricated using the process parameters of the first pass and the second pass, respectively. D denotes the average depth of the microchannel in the region between the centers of the first and second passes, O and O'.

Ideally, the microchannel fabricated should have a complete flat region between O and O', which is an ideal trapezoid shape. However, in the real process, this cannot be achieved due to the surface roughness caused by laser ablation and resolidfication of PMMA. In order to determine how close the fabricated microchannel is to the ideal trapezoidal microchannel quantitatively, a quality index Q is introduced. Q is calculated using Eq. 4, which has a definition similar to the surface roughness parameter Ra:

$$Q = \frac{\sum |D_i - D|}{n} \tag{4}$$

where D_i is the depth measured in the bottom region and n is the number of data points at the bottom region. The fabricated microchannel that has the closest ideal groove shape should have the minimum Q value.

Figure 5 summarizes the input process parameters of the two-pass fabrication method and the resultant microchannel dimensional parameters as output. There are totally five process parameters: laser power and line energy for the first and second passes, P_1, E_1 and P_2, E_2, and the offset ratio controlled by the X-Y table. Three main output dimensional parameters are used to characterize the microchannel: width W, average depth D, and quality index Q.

3.3 The optimized offset ratio

It was observed that the trapezoidal grooved microchannel can be fabricated by using an offset ratio ranging from 45 to 55%. Figures 6, 7, and 8 show the microchannels fabricated using an offset ratio of 45, 50, and 55%, respectively. The laser power of the first and second passes is 4 W. The scanning speed of the first pass is 25 mm/s, while the second pass line energies are 37.88, 38.46, and 35.7 mm/s at the offset ratio of 45, 50, and 55%, respectively. The width, depth, and quality index Q of the microchannel are reported in Table 3. The groove profiles are compared against the groove shape fabricated after the first pass.

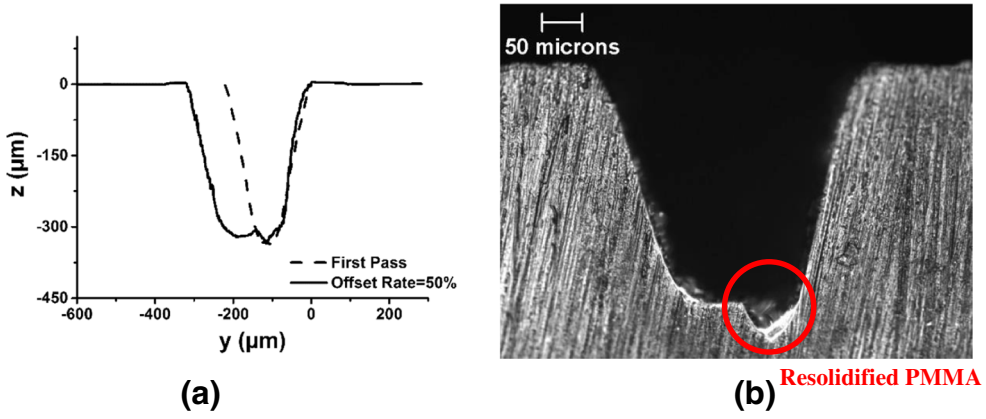

Fig. 7 Groove profile of a microchannel fabricated by two-pass scanning using $P_1 = P_2 =$ 4 W $E_1 = 160$J/m $E_2 = 104$J/m Offset ratio = 50% measured by **a** 3D optical microscope and **b** optical microscope

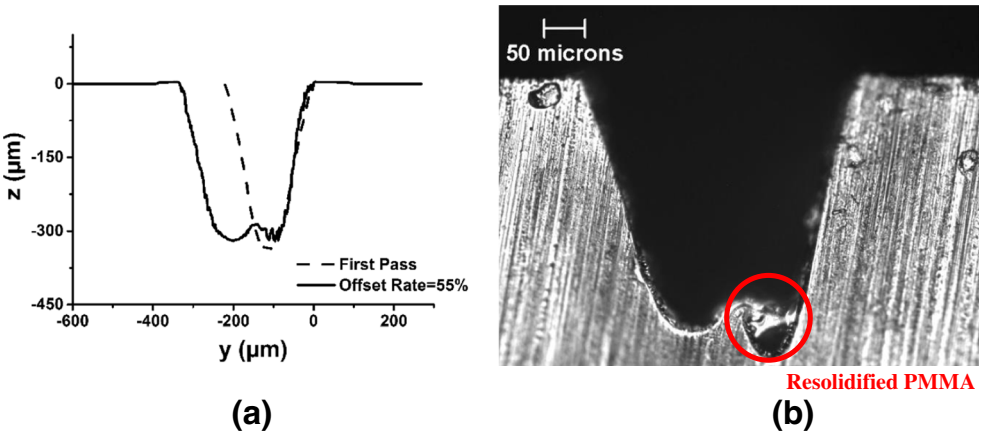

Fig. 8 Groove profile of a microchannel fabricated by two-pass scanning using $P_1 = P_2 =$ 4 W $E_1 = 160$J/m $E_2 = 112$J/m Offset ratio = 55% measured by **a** 3D optical microscope and **b** optical microscope

Figure 9 illustrates the laser micromachining process of the second pass scanning for the beam spot size region at the offset ratio of 45, 50, and 55%. During the second pass, the microchannel wall against the offset direction hardly absorbs the CO_2 laser beam and no material melts or vaporizes in that region. On the other side, the PMMA experiences photothermal melting and evaporation. At the rim of the beam spot near the first scanning center, where the line energy density is relatively low, the PMMA is instantly melted and ejected out of the local region by the high pressure of the hot evaporated gas. The molten PMMA is then deposited and subjected to cooling at the valley created by the first pass. At the offset ratio of 55% (Fig. 9b), there is a big low line energy density region between the first and second scanning centers, and thus a large amount of PMMA is solidified at the valley as shown by Fig. 8. Both the ablation and redeposition effects make a near trapezoidal groove shape microchannel with a hump at the bottom. Thus, the depth of the microchannel is smaller than the depth fabricated by the first pass scanning and Q is relatively high. When the offset ratio equals 50% (Fig. 9c), still some PMMA is solidified at the valley, but the solidification effect is smaller as shown in Fig. 7. This is attributed to the fact that the line energy density region between the first and second scanning centers is smaller. At the offset ratio of 45% (Fig. 9d), the high line energy density region of the two passes overlaps. The ejected PMMA is further vaporized by the CO_2 laser irradiation, which makes the wall against the offset direction hardly affected. This offset ratio will result in a clean cut of the second pass and let the microchannel maintain the depth fabricated by the first pass. As shown in Fig. 6, the quality index at the offset ratio of 45% is low and the difference between the depth of the microchannel fabricated before and after the second pass is only 1.4 μm.

As shown by Fig. 6, by using the offset ratio of 45%, the cross section shape of the microchannel fabricated is close to an ideal trapezoid shape. Also, no PMMA is resolidified in this process. In CO_2 laser microchanneling, the resolidification and clogging are the defects that should be avoided. By using the offset ratio of 45%, these defects can be avoided. Therefore, the offset ratio of 45% is used in the two-pass fabrication method and depth D should be equal to the microchannel depth fabricated by the first pass D_1.

3.4 The optimized line energy ratio at the offset ratio of 45%

It was found that when the offset ratio is equal to 45%, a trapezoidal grooved microchannel can be fabricated if the ratio between line energy of the second pass and that of the first pass remains constant, where the constant is a function of first-pass line energy E_1. This relationship can be further explored by Figs. 10 and 11. Figure 10 shows the quality index values of the microchannels fabricated using the first-pass laser power P_1 of 4 W and the first-pass line energy E_1 of 160 mm/s with the offset ratio of 45%. The laser power of the second pass P_2 varied from 2 to 10 W while maintaining E_2/E_1 equal to 0.66. It can be observed from Fig. 10 that the quality index value is smaller than 4 μm for different P_2 and U_2 that satisfied E_2/E_1 equal

Table 3 Dimensional parameters for microchannel fabricated using different offset rates

No.	$P_1 = P_2$ (W)	E_1 (J/m)	E_2 (J/m)	Offset ratio	W (μm)	D (μm)	Q (μm)
1	4	160	105.6	45%	313.9 ± 1.6	340.4 ± 2.5	1.7 ± 0.4
2			104	50%	319.0 ± 2.2	316.6 ± 4.7	3.8 ± 0.7
3			112	55%	333.6 ± 1.7	302.9 ± 8.2	11.3 ± 3.7

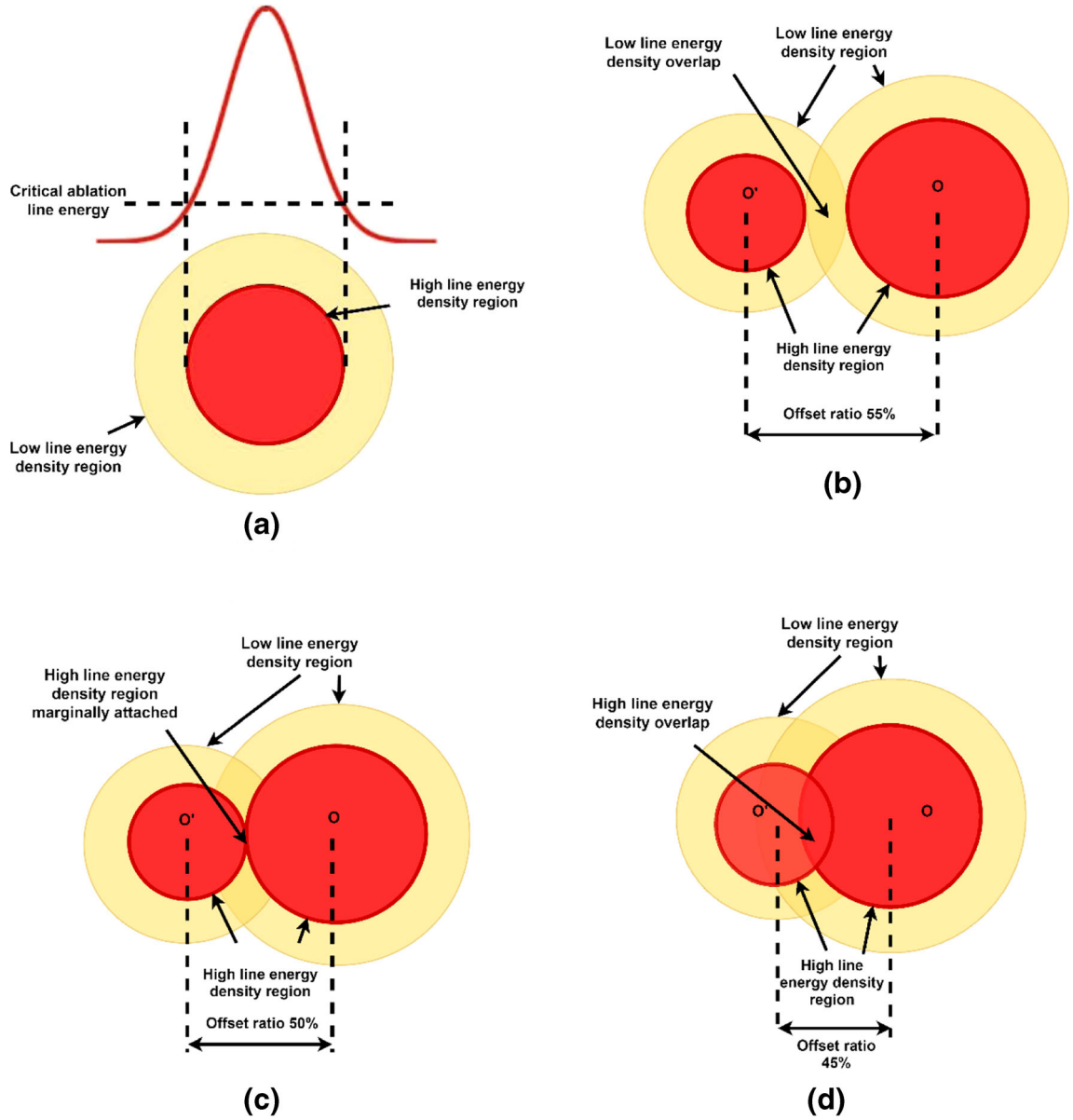

Fig. 9 Illustration of the **a** high and low line energy density region and the laser micromachining process of the second pass scanning for the beam at the offset ratio of **b** 55%, **c** 50%, and **d** 45%

to 0.66 when E_1 is 160 J/m. Figure 11 compares the depth of these microchannels fabricated by two-pass ablation with the depth generated by the first pass. From Fig. 11, it can be seen that the depth of each microchannel fabricated by two passes is within 5 μm difference from D_1. This indicates that a flat microchannel bottom can be made for a wide range of laser parameters as long as the E_2/E_1 ratio is kept at 0.66 when E_1 is 160 J/m.

Figures 12 and 13 show the groove profiles of the microchannel using P_2 of 2 and 6 W at the offset ratio of 45%. It can be observed that the microchannels have well-developed trapezoid shapes and are of higher quality. The results indicate that as long as E_1 and E_2 meet the requirement, a high-quality trapezoidal microchannel can be fabricated by the two-pass fabrication method.

In order to find the exact relationship between E_1 and E_2 that will yield a high-quality microchannel, experiments were conducted at various first-pass line energy levels of 80, 160, 240, and 320 J/m. At 80 J/m, P_1 of 4 W was selected to be investigated. P_1 of 6 W was chosen for the first-pass line energy of 160 and 240 J/m. P_1 of 8 W was selected for E_1 equal to 320 J/m. The line energies of the second pass at four different first-pass line energy levels were achieved by changing the second pass scanning speed alone while remaining the second pass laser power the same as the first pass.

Figures 14 and 15 show the quality index value and D/D_1 of the microchannel fabricated using different line

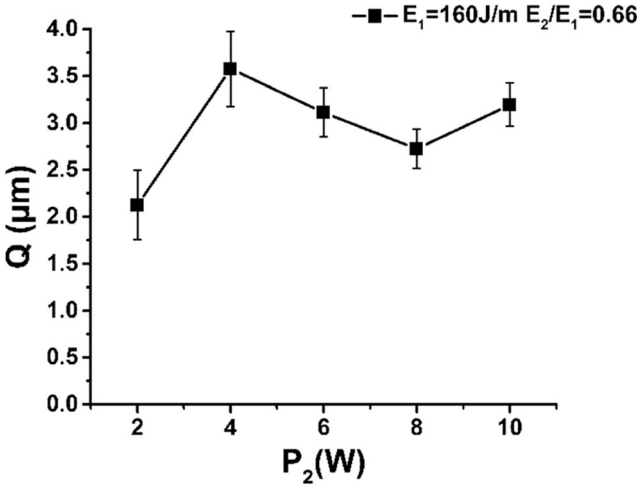

Fig. 10 Variation of the quality index value with the second-pass laser power P_2 for the first-pass laser power P_1 of 4 W and line energy E_1 of 160 J/m with line energy ratio of 0.66

energy E_2/E_1 ratios at four E_1 levels. It is observed that for the first pass-line E_1 energies of 80, 160, 240, and 320 J/m, the corresponding optimized line energy ratios are 0.63, 0.66, 0.68, and 0.7, respectively, which will yield microchannels of the best quality, namely, having a more trapezoid shape and a microchannel depth closest to D_1.

The line energy ratio that will yield the best-quality microchannel in terms of the line energy of the first pass can be obtained by using linear regression as expressed by Eq. 5.

$$\frac{E_2}{E_1} = 0.0003E_1 + 0.61 \tag{5}$$

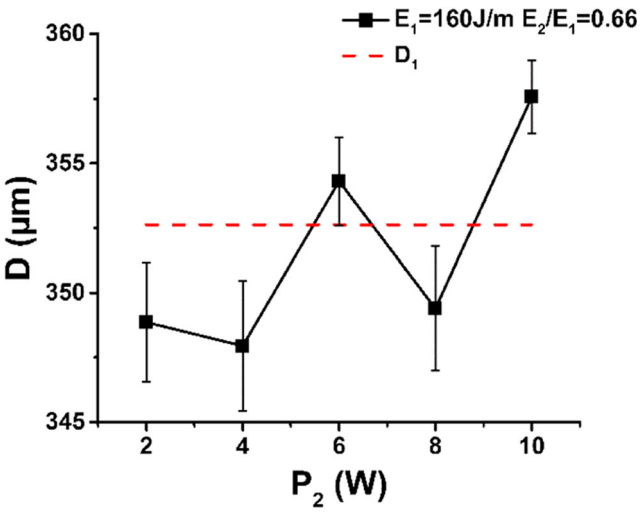

Fig. 11 Variation of microchannel depth with the second-pass laser power P_2 for the first-pass laser power P_1 of 4 W and line energy E_1 of 160 J/m with line energy ratio of 0.66

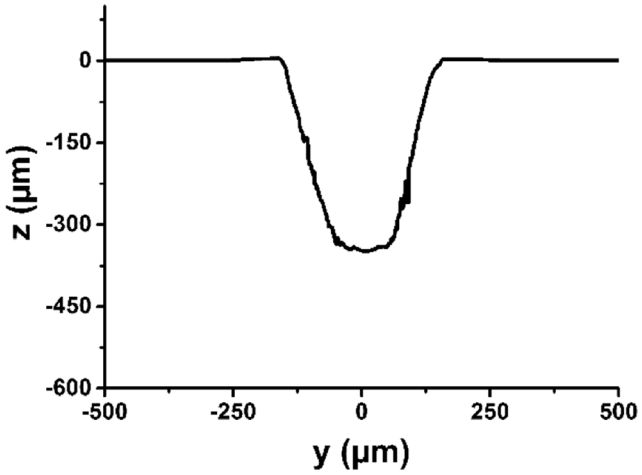

Fig. 12 Groove profile of a microchannel fabricated by two-pass scanning using $P_1 = 4$ W $P_2 = 2$ W $E_1 = 160$J/m $E_2 = 105.6$J/m Offset ratio = 45% measured by 3D optical microscope

4 Developed regression model for fabricating the trapezoidal microchannel of arbitrary dimensions

4.1 Regression model for single pass

In order to determine the process parameters to be used for fabricating the trapezoidal microchannel with the arbitrary desired dimensions, regression models for single passes fabricated were first developed. The line energy used in the investigation ranges from 35 to 320 J/m with seven levels in total. Three levels of line energy were chosen in the range from 35 to 65 J/m with an increment of 15 J/m. At the line energy of 35 J/m, the laser power levels of 2 and 4 W were investigated. The laser power of 2, 4, and 6 W were tested when the line energy equals 50 J/m. Four levels of laser power ranging from 2 to 8 W were explored at the line energy of 65 J/

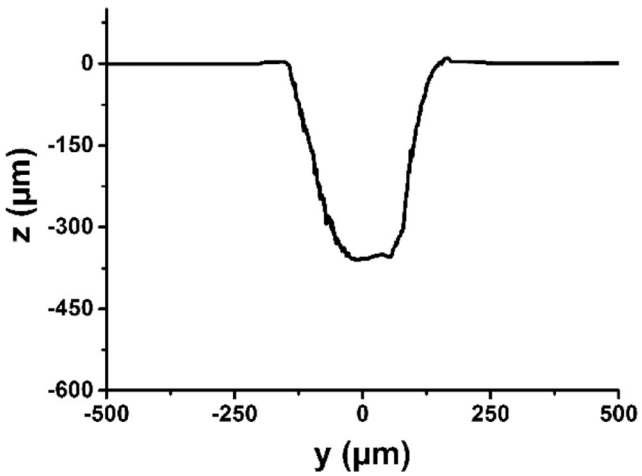

Fig. 13 Groove profile of a microchannel fabricated by two-pass scanning using $P_1 = 4$ W $P_2 = 6$ W $E_1 = 160$J/m $E_2 = 105.6$J/m Offset ratio = 45% measured by 3D optical microscope

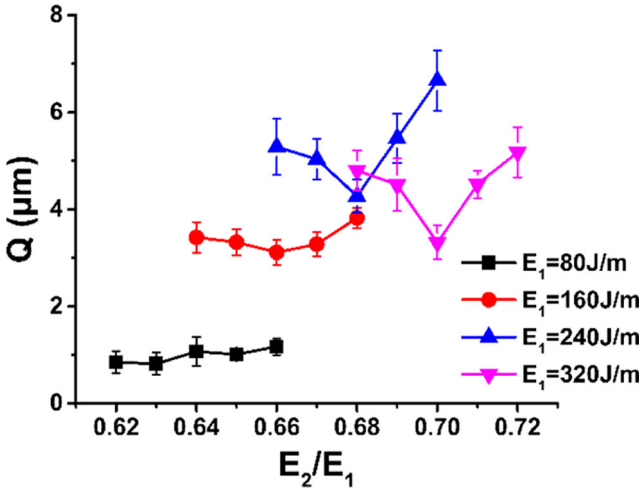

Fig. 14 Variation of quality index value with line energy ratio for the first-pass line energies of 80, 160, 240, and 320 J/m

m. In the range from 80 to 320 J/m, four levels of line energy were selected with the increment of 80 J/m. Five levels of laser power, which vary from 2 to 10 W, are investigated in this range. The selected laser power and line energy levels are shown in Table 4. The corresponding scanning speed can be determined using Eq. 2. The measurements results of 29 sets of experiments are reported in Table 5.

Based on the experimental results, regression models were constructed to describe the relationship between the dimensional parameters and the process parameters. The dimensional parameters have a nonlinear relationship with line energy and laser power. To simplify this nonlinear relationship, the models are built using the form in Eq. 6. To make it easier to find the process parameters for fabricating the microchannel of a desired dimension, product terms were used.

$$F(P,E) = KP^{\alpha}E^{\beta}ln(P)^{\gamma}ln(E)^{\delta} \tag{6}$$

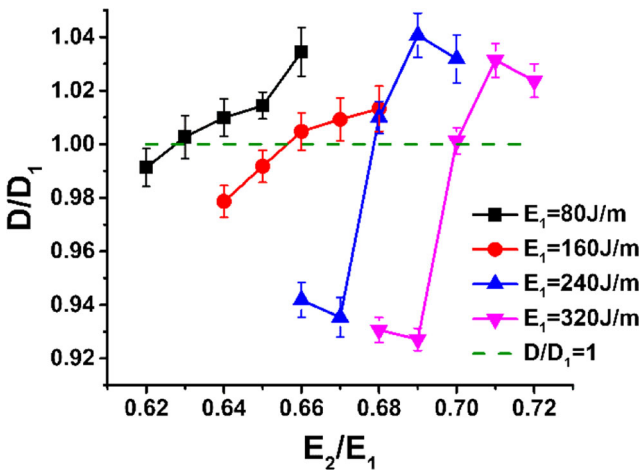

Fig. 15 Variation of D/D_1 with line energy ratio for the first-pass line energies of 80, 160, 240, and 320 J/m

Table 4 Selected laser power and line energy for the designed experiments

		Line energy levels (J/m)						
		35	50	65	80	160	240	320
Power levels (W)	2	●	●	●	●	●	●	●
	4	●	●	●	●	●	●	●
	6	○	●	●	●	●	●	●
	8	○	○	●	●	●	●	●
	10	○	○	○	●	●	●	●

● Performed, ○ not performed

By taking the natural log of Eq. 6 on both sides, the nonlinear mathematical models are transformed into a linear relationship as shown in Eq. 7.

$$ln(F) = ln(K) + \alpha ln(P) + \beta ln(E) + \gamma ln(ln(P)) + \delta ln(ln(E)) \tag{7}$$

Models were then built using a linear regression analysis. The analysis-of-variance (ANOVA) table of the model for the width of the microchannel is given in Table 6 using the log value of each parameter. The P value of the model is less than 0.05 (95% confidence level), which indicates that the modeling terms are statistically significant. In the linearized equation form, the term ln(ln(P)) was not statistically significant and was eliminated by a backward elimination process. The adequacy indices for the model like R^2, adjusted R^2, and predicted R^2 are all close to 1, which indicates the validity of the model. For the microchannel depth, the adequacy measures, R^2, adjusted R^2, and predicted R^2, all suggest the adequacy of the model. Table 7 presents the ANOVA table of the model for the depth. The associated P values of each term are less than 0.05 (95% confidence level), which shows statistical significance. The term ln(E) in the linearized equation form is of low statistical significance and thus eliminated by a backward elimination process to improve the model adequacy. The final regression models for microchannel width and depth in the nonlinear equation form are given by Eqs. 8 and 9, respectively.

$$W = 17.29P^{-0.019}E^{-0.28}ln(E)^{2.45} \tag{8}$$

$$D = 0.143P^{0.28}ln(P)^{-0.36}ln(E)^{4.63} \tag{9}$$

The adequacy of the models was first examined by comparing the predicted values of the channel depth and the channel width with experimental data reported in Table 5. Figures 16 and 17 show the relationships between the actual values and predicted values of the channel depth and channel width, respectively. For the model of width, the average

Table 5 Experimental results for the single-pass grooving

No.	Process parameters			Results	
	P (W)	*U* (mm/s)	*E* (J/m)	*D* (μm)	*W* (μm)
1	2	57.14	35	74.1 ± 2.1	141.6 ± 1.1
2	2	40.00	50	109.1 ± 1.6	162.6 ± 0.6
3	2	30.77	65	152.2 ± 4.3	176.4 ± 2.3
4	2	25.00	80	191.6 ± 2.6	191.5 ± 0.7
5	2	12.50	160	353.8 ± 6.7	223.4 ± 4.7
6	2	8.33	240	506.0 ± 5.9	235.3 ± 2.9
7	2	6.25	320	596.7 ± 6.3	250.0 ± 3.3
8	4	114.29	35	66.6 ± 1.7	143.2 ± 1.7
9	4	80.00	50	102.2 ± 1.9	160.1 ± 1.6
10	4	61.54	65	138.0 ± 3.1	168.7 ± 1.1
11	4	50.00	80	175.0 ± 3.2	187.2 ± 3.1
12	4	25.00	160	339.3 ± 3.7	221.1 ± 1.7
13	4	16.67	240	481.9 ± 4.7	237.7 ± 2.2
14	4	12.50	320	618.0 ± 6.3	248.3 ± 3.2
15	6	120.00	50	102.1 ± 3.3	159.4 ± 1.6
16	6	92.31	65	137.8 ± 0.9	167.4 ± 1.6
17	6	75.00	80	180.3 ± 1.0	184.2 ± 1.2
18	6	37.50	160	354.9 ± 1.2	219.8 ± 0.9
19	6	25.00	240	516.8 ± 3.5	234.6 ± 2.8
20	6	18.75	320	671.0 ± 6.5	248.7 ± 1.4
21	8	123.08	65	136.3 ± 1.9	167.5 ± 3.3
22	8	100.00	80	176.1 ± 2.6	189.0 ± 2.6
23	8	50.00	160	353.3 ± 2.4	216.3 ± 2.4
24	8	33.33	240	512.6 ± 7.1	234.7 ± 1.5
25	8	25.00	320	675.8 ± 7.4	241.8 ± 3.1
26	10	125.00	80	183.8 ± 2.2	186.2 ± 1.1
27	10	62.50	160	363.6 ± 2.1	215.5 ± 3.1
28	10	41.67	240	531.5 ± 4.5	232.8 ± 2.2
29	10	31.25	320	697.1 ± 7.5	239.9 ± 2.1

absolute error is 2.0 μm and the error for the point is within 3.5% of the actual microchannel width. The average absolute error for the depth model is 9.5 μm. The results show that the mathematical models are adequate.

To further test the viability of the developed models, four confirmation experiments were conducted with laser operating conditions chosen randomly in the range where the mathematical models are derived. The actual values, predicted

Table 6 ANOVA analysis for the microchannel width

Source	Degrees of freedom	Sum of squares	Mean squares	*F* value	*P* value
Model	3	0.8841	0.2947	1119.92	<0.001
ln(*P*)	1	0.0029	0.0029	11.18	0.003
ln(*E*)	1	0.0045	0.0045	16.99	<0.001
ln(ln(*E*))	1	0.0155	0.0155	58.91	<0.001
Pure error	25	0.0066	0.0003		
Total	28	0.8906			

R^2 = 99.26%, adjusted R^2 = 99.17%, predicted R^2 = 99.00%

Table 7 ANOVA analysis for the microchannel depth

Source	Degrees of freedom	Sum of squares	Mean squares	*F* value	*P* value
Model	3	15.0215	5.0072	3742.27	<0.001
ln(*P*)	1	0.0184	0.0184	13.74	0.001
ln(ln(*P*))	1	0.0186	0.0186	13.89	0.001
ln(ln(*E*))	1	13.6035	13.6035	10,167	<0.001
Pure error	25	0.0335	0.0013		
Total	28	15.0550			

R^2 = 99.78%, adjusted R^2 = 99.75%, predicted R^2 = 99.68%

values, and percentage error are presented in Table 8. It can be observed that there is low percentage error (less than 3.0%) between the predicted and actual values. This indicates validity of the developed models. Also, this nonlinear model has a better accuracy than the model derived by Prakash et al., which has percentage errors larger than 3% [11].

4.2 Process parameter determination of the two-pass fabrication method

In the two-pass fabrication method, the trapezoid microchannel will have the same depth as the depth of the microchannel fabricated by the first pass when using the offset ratio of 45%. Thus, the process parameters of the first pass should meet the requirement as depicted by Eq. 10.

$$D(P_1, E_1) = D_{\text{target}} \tag{10}$$

where D_{target} is the desired microchannel depth. In addition, the width of the microchannel fabricated by the two-pass fabrication method can be estimated by Eq. 3 when the 45% offset ratio is used. Thus, the process parameters should meet the relationship shown in Eq. 11.

$$0.95W(P_1, E_1) + 0.5W(P_2, E_2) = W_{\text{target}} \tag{11}$$

where W_{target} is the desired microchannel width.

In order to fabricate a symmetric microchannel, the process parameters of the first and second passes should also meet the requirement such that

$$W(P_2, E_2) = W(P_1, E_1) \tag{12}$$

However, in most cases, this requirement cannot be achieved. This is because the line energy of the second pass is smaller than the first pass' line energy which is constrained by Eq. 5. Thus, in most cases, $W_2 < W_1$. In order to fabricate the microchannel of the highest symmetricity, lower laser power should be chosen since the width of the microchannel is a monotonically decreasing function of laser power at a fixed line energy level as shown by Eq. 8. In this study, the laser power of 2 W was chosen if the relationship of Eq. 12 cannot be achieved. In addition, the line energy ratio should meet the requirement given by Eq. 5. Thus, the process parameters can be obtained by solving the following group of equations:

$$W_{\text{target}} = 0.95W(P_1, E_1) + 0.5W(P_2, E_2) \tag{13.a}$$

$$D_{\text{target}} = D(P_1, E_1) \tag{13.b}$$

$$\frac{E_2}{E_1} = 0.0003E_1 + 0.61 \tag{13.c}$$

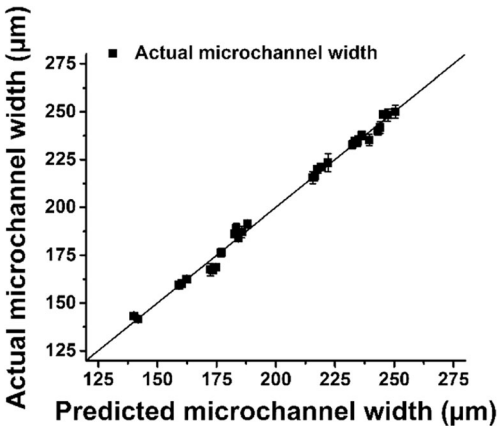

Fig. 16 Plot of actual vs. predicted channel width

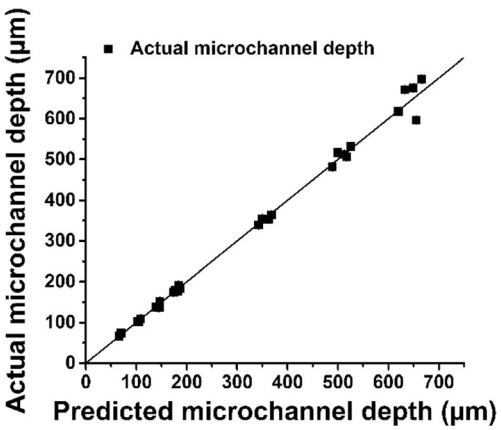

Fig. 17 Plot of actual vs. predicted channel depth

Table 8 Experiments results of confirmation for single-pass scanning

No.	P (W)	E (J/m)		W (μm)	D (μm)
1	4	280	Actual	237.6 ± 2.7	564.9 ± 6.4
			Predicted	240.3	561.6
			Error %	1.2%	0.6%
2	6	200	Actual	223.3 ± 1.4	433.9 ± 5.3
			Predicted	225.3	431.3
			Error %	0.9%	0.6%
3	2	120	Actual	209 ± 1.3	272.3 ± 2.2
			Predicted	207.1	279.1
			Error %	0.9%	2.5%
4	2.5	60	Actual	168.7 ± 1.8	133.2 ± 2.7
			Predicted	170.7	130.3
			Error %	1.2%	2.2%

Table 9 Experiments results of confirmation for two-pass scanning

No.	P_1 (W)	E_1 (J/m)	P_2 (W)	E_2 (J/m)	Q (μm)		W (μm)	D (μm)
1	8	120	8	77.5	1.9 ± 0.3	Actual	284.4 ± 2.3	262.6 ± 4.6
						predicted	281.7	274.1
						error %	0.9%	4.4%
2	10	320	2	226	3.1 ± 0.6	Actual	349.9 ± 2.8	690.9 ± 7.1
						predicted	346.4	673.9
						error %	1.0%	2.5%

Two confirmation experiments were conducted with fabrication conditions randomly selected to further test the viability of Eq. 13. The process parameters and dimensional values are reported in Table 9. The predicted values of microchannel depth and width are also compared with actual values and percentage errors. Figures 18 and 19 show the groove profiles of the microchannels. It can be observed that the microchannels are of higher quality and they have a high degree of bottom flatness. The widths and depths of the microchannels have a good agreement with the predicted values, which indicates the viability of Eq. 13.

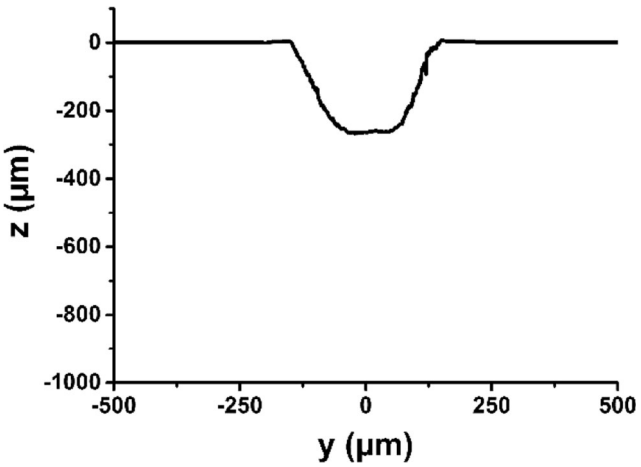

Fig. 18 Groove profile of a microchannel fabricated by two-pass scanning using $P_1 = 8$ W $P_2 = 8$ W $E_1 = 120$J/m $E_2 = 77.5$J/m Offset ratio = 45% measured by a 3D optical microscope

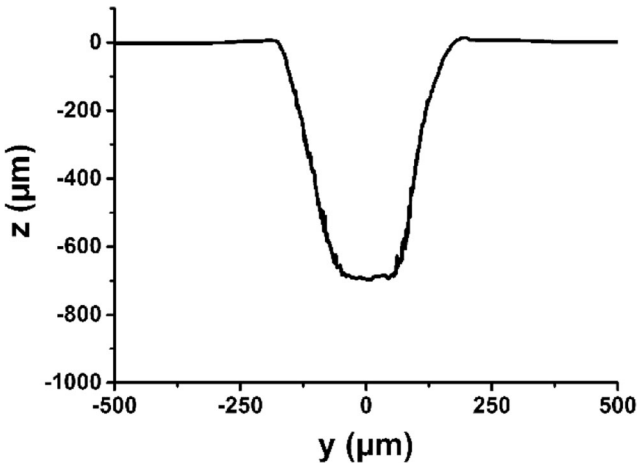

Fig. 19 Groove profile of a microchannel fabricated by two-pass scanning using $P_1 = 10$W $P_2 = 2$W $E_1 = 320$J/m $E_2 = 226$J/m Offset ratio = 45% measured by a 3D optical microscope

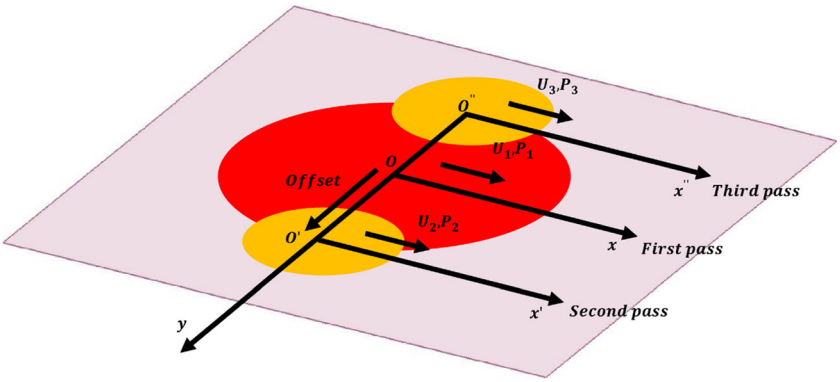

Fig. 20 Illustration of a three-pass fabrication method

Table 10 Experiments results of confirmation for three-pass scanning

No.	P_1 (W)	E_1 (J/m)	$P_2 = P_3$ (W)	$E_2 = E_3$ (J/m)	Q (μm)		W (μm)	D (μm)
1	10	225	8	152.6	1.9 ± 0.4	Actual	418.1 ± 2.4	494.3 ± 6.8
						predicted	420	500
						Error %	0.5%	1.2%

The two-pass fabrication method can be extended to a three-pass fabrication process to solve the problem of asymmetricity and to fabricate a wider microchannel. This method is illustrated by Fig. 20. The microchannel is fabricated by three-pass laser ablation. O, O', and O'' are the centers of the first second and third passes, respectively. The second and third passes have the same offset of 45% W_1 with different directions from the first pass. The process parameters of the second pass and the third pass are the same. The width of the microchannel can be estimated by Eq. 14.

$$W = 0.9W_1 + W_2 \tag{14}$$

Thus, the process parameters can be obtained by solving the following group of equations:

$$P_2 = P_3, U_2 = U_3 \tag{15.a}$$

$$W_{\text{target}} = 0.9W_1 + W_2 \tag{15.b}$$

$$D_{\text{target}} = D(P_1, E_1) \tag{15.c}$$

$$\frac{E_2}{E_1} = 0.0003E_1 + 0.61 \tag{15.d}$$

To test the viability of Eq. 15, one confirmation experiment was conducted. Table 10 shows the process parameters selected for fabricating a microchannel. The groove profile of the microchannel is shown in Fig. 21. The microchannel has a width of 418.1 μm and a depth of 494.3 μm with a quality index value of only 2.8 μm. It can thus be observed that the microchannel is symmetric and of high quality. This indicates the adequacy of Eq. 15.

5 Flow test of the trapezoidal microchannel

From previous research, it was found that a trapezoidal microchannel is superior to a triangular microchannel of the same cross section area. In order to compare the performance of the two microchannels, a PMMA-based microfluidic chip with two parallel microchannels of 3 mm length was fabricated. One of the microchannels was fabricated using the conventional single-pass fabrication method using the laser power of 8 W and line energy of 320 J/m. The microchannel has a triangular cross section shape with a depth of 675.8 μm and a width of 241.8 μm as shown by Fig. 22. The other microchannel was fabricated using the two-pass fabrication method. In the first pass, power of 6 W and line energy of

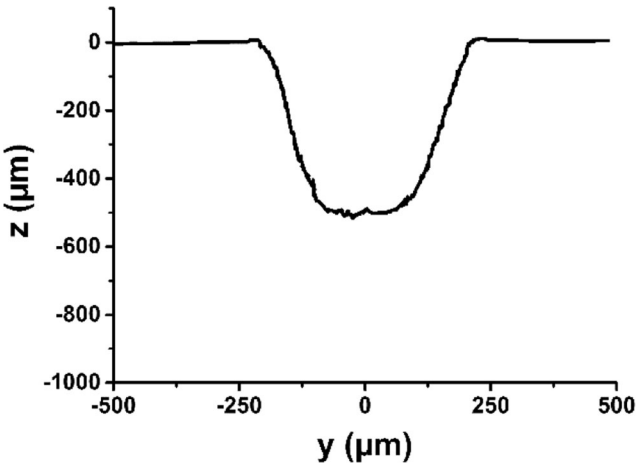

Fig. 21 Groove profile of a microchannel fabricated by two-pass scanning using $P_1 = 10$W $P_2 = P_3 = 2$W $E_1 = 225$ J/m $E_2 = E_3 = 152.6$ J/m Offset ratio = 45% measured by a 3D optical microscope

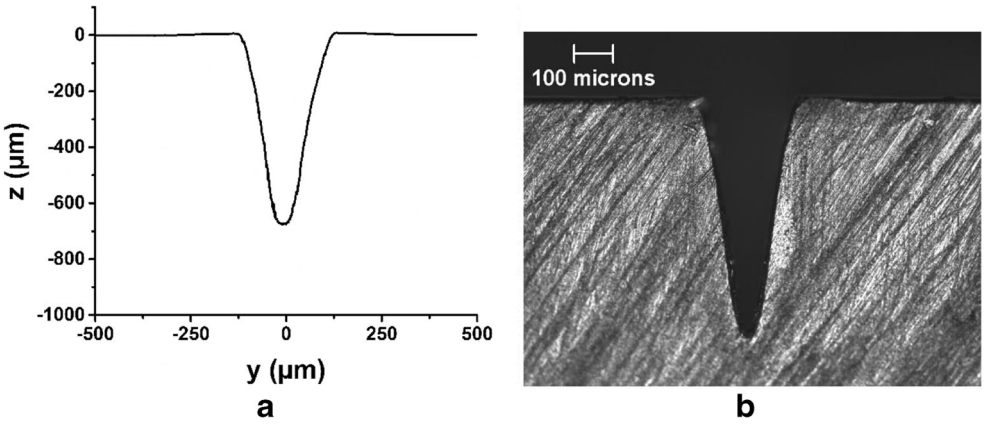

Fig. 22 Groove profile of a microchannel fabricated by one-pass scanning with $P = 8$ W $E = 320$ J/m measured by **a** 3D optical microscope and **b** optical microscope

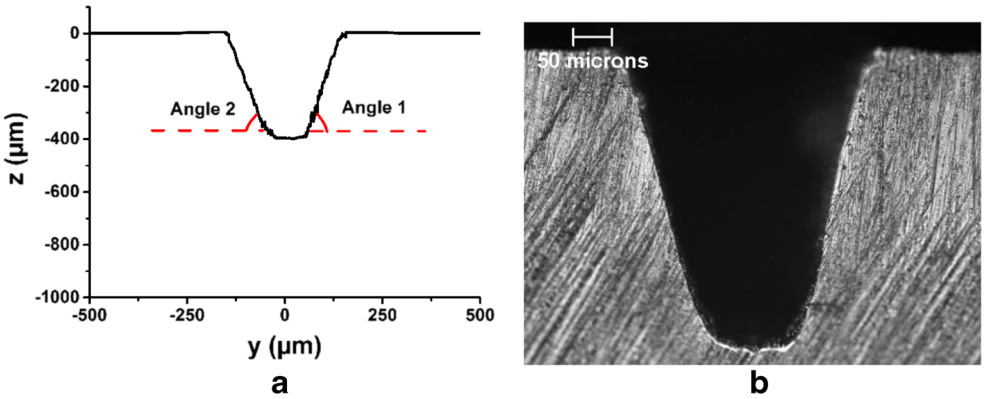

Fig. 23 Groove profile of a microchannel fabricated by two-pass scanning using $P_1 =$ 6W $P_2 = 2$W $E_1 = 186.3$J/m $E_2 =$ 124.1J/m Offset ratio = 45% measured by **a** 3D optical microscope and **b** optical microscope

186.3 J/m were used. In this case, the relationship of Eq. 12 cannot be achieved and thus 2 W is used for the second-pass laser power with the corresponding line energy of 124.1 J/m. The microchannel has a width of 309.2 μm and a depth of 397.2 μm as shown by Fig. 23. The quality index value is 1.9 μm. For the degree of symmetricity, the wall on the first-pass center side (angle 1) has an angle of 76.2°, while the wall on the second-pass center side (angle 2) has an angle of 74.8°. The difference is only 1.4°, which indicates that the asymmetricity can be neglected. The cross sectional area of the triangular microchannel is 0.0822 m^2 while the cross section area of the trapezoidal microchannel is 0.0825 m^2. The difference is within 0.36%.

To compare the pressure drop of the microchannels, a syringe pump system was constructed as shown by Fig. 24. The syringe was used to provide the flow of the same pressure head for the microchannels. Two chambers were used to collect the fluid flow through different microchannels. The feeding needles used to feed the flow have a diameter of 250 μm. The syringe fed the flow at a flow rate of 1 mL/min, and the syringe pump was operated for 4 min at a time. The flow rates through the microchannels are determined by measuring the weight change of the water chambers.

The PMMA substrates were thermally bonded using a hot plate. A thermal bonding process similar to the one developed by Sun et al. [19] was used. The substrates were first cleaned with deionized water by an ultrasonic cleaner for 5 min and then dried using high-pressure air. The bonding pressure was 11 kPa. The substrates were first heated up to 155 °C for 10 min and then maintained at that temperature for 45 min. The bonded chip was then cooled down to 80 °C for 20 min and annealed at this temperature for 20 min to relieve the stresses. Finally, it was cooled down to room temperature for 20 min. The thermal cycle

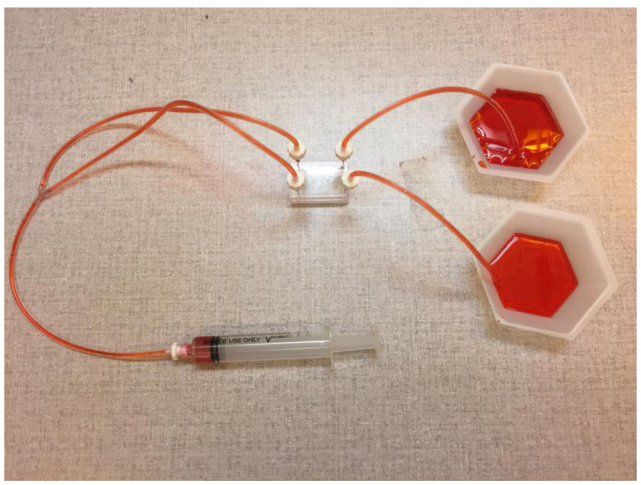

Fig. 24 The syringe pump system for testing microchannel performance

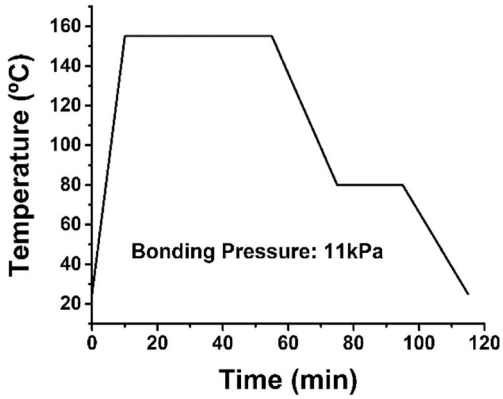

Fig. 25 Thermal cycle for the bonding of PMMA substrates

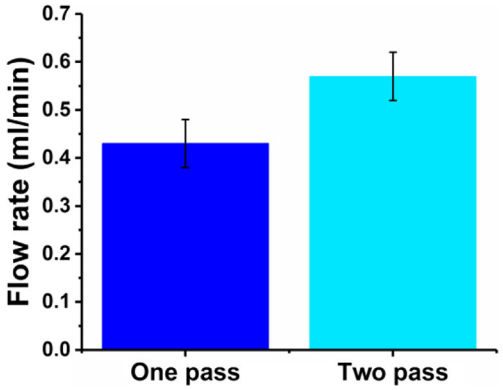

Fig. 27 The resultant flow rates of the triangular and trapezoidal microchannel

for the bonding is demonstrated by Fig. 25. The cross sections of the microchannels after thermal bonding are shown by Fig. 26. It can be observed that the microchannels are hardly affected by the thermal bonding process.

The resultant flow rate of the triangular microchannel was 0.43 mL/min while the trapezoidal microchannel yielded a flow rate of 0.57 mL/min, which is 32.6% higher. This is because the triangular microchannel has a larger perimeter that yields a larger friction force. Thus, it can be concluded that the trapezoidal microchannel is more desirable (Fig. 27).

6 Conclusion

CO_2 laser-based microchanneling of PMMA using a two-pass fabrication method was investigated in this paper. This method can provide a rapid and economic way of fabricating higher-performance trapezoidal microchannels on various PMMA-based microfluidic devices. The key conclusions are listed below:

- It was found that at the offset ratio of 45%, clogging and resolidification effects can be avoided and it will yield a clean cut.
- A trapezoidally grooved microchannel can be fabricated if the ratio between the line energy of the second pass and that of the first pass remains constant, which is a function of the first-pass line energy E_1. The empirical relationship between line energy ratio and the first-pass line energy can be depicted as

$$\frac{E_2}{E_1} = 0.0003E_1 + 0.61$$

- Nonlinear regression models with high accuracy were derived to predict the width and depth of the microchannel fabricated by a single pass:

$$W = 17.29P^{-0.019}E^{-0.28}\ln(E)^{2.45}$$
$$D = 0.143P^{0.28}\ln(P)^{-0.36}\ln(E)^{4.63}$$

- Two groups of equations were established to determine the process parameters that can be used in two-pass and three-pass fabrication of a microchannel of any desired dimensions.

Fig. 26 Profile of the **a** triangular and **b** trapezoidal microchannels after thermal bonding

- The performances of the triangular and trapezoidal microchannels with the same cross sectional area were compared on a microfluidic chip. The results showed that the trapezoidal microchannel yielded a higher flow rate under the same pressure head.

References

1. Prakash S, Kumar S (2015) Fabrication of microchannels: a review. Proc Inst Mech Eng B J Eng Manuf 229(8):1273–1288
2. Hong TF, Ju WJ, Wu MC, Tai CH, Tsai CH, Fu LM (2010) Rapid prototyping of PMMA microfluidic chips utilizing a CO2 laser. Microfluid Nanofluid 9(6):1125–1133
3. Becker H, Gärtner C (2008) Polymer microfabrication technologies for microfluidic systems. Anal Bioanal Chem 390(1):89–111
4. Chen PC, Pan CW, Lee WC, Li KM (2014) An experimental study of micromilling parameters to manufacture microchannels on a PMMA substrate. Int J Adv Manuf Technol 71(9–12):1623–1630
5. Klank H, Kutter JP, Geschke O (2002) CO2-laser micromachining and back-end processing for rapid production of PMMA-based microfluidic systems. Lab Chip 2(4):242–246
6. Snakenborg D, Klank H, Kutter JP (2003) Microstructure fabrication with a CO2 laser system. J Micromech Microeng 14(2):182
7. Prakash S, Kumar S (2015) Profile and depth prediction in single-pass and two-pass CO2 laser microchanneling processes. J Micromech Microeng 25(3):035010
8. Xiang, H., Fu, J., & Chen, Z. (2006). 3D finite element modeling of laser machining PMMA. In: 2006 1st IEEE International Conference on Nano/Micro Engineered and Molecular Systems (pp. 942–946). IEEE.
9. Romoli L, Tantussi G, Dini G (2011) Experimental approach to the laser machining of PMMA substrates for the fabrication of microfluidic devices. Opt Lasers Eng 49(3):419–427
10. Chung CK, Lin SL (2011) On the fabrication of minimizing bulges and reducing the feature dimensions of microchannels using novel CO2 laser micromachining. J Micromech Microeng 21(6):065023
11. Chung CK, Tu KZ (2014) Application of metal film protection to microfluidic chip fabrication using CO2 laser ablation. Microsyst Technol 20(10–11):1987–1992
12. Li JM, Liu C, Zhu LY (2009) The formation and elimination of polymer bulges in CO2 laser microfabrication. J Mater Process Technol 209(10):4814–4821
13. Nayak NC, Lam YC, Yue CY, Sinha AT (2008) CO2-laser micromachining of PMMA: the effect of polymer molecular weight. J Micromech Microeng 18(9):095020
14. Huang Y, Liu S, Yang W, Yu C (2010) Surface roughness analysis and improvement of PMMA-based microfluidic chip chambers by CO 2 laser cutting. Appl Surf Sci 256(6):1675–1678
15. Kurnia JC, Sasmito AP, Birgersson E, Shamim T, Mujumdar AS (2014) Evaluation of mass transport performance in heterogeneous gaseous in-plane spiral reactors with various cross-section geometries at fixed cross-section area. Chem Eng Process Process Intensif 82:101–111
16. Gunnasegaran P, Mohammed HA, Shuaib NH, Saidur R (2010) The effect of geometrical parameters on heat transfer characteristics of microchannels heat sink with different shapes. Int Commun Heat Mass Transf 37(8):1078–1086
17. Bhuyan MK, Courvoisier F, Lacourt PA, Jacquot M, Furfaro L, Withford MJ, Dudley JM (2010) High aspect ratio taper-free microchannel fabrication using femtosecond Bessel beams. Opt Express 18(2):566–574
18. Darvishi S, Cubaud T, Longtin JP (2012) Ultrafast laser machining of tapered microchannels in glass and PDMS. Opt Lasers Eng 50(2):210–214
19. Sun Y, Kwok YC, Nguyen NT (2006) Low-pressure, high-temperature thermal bonding of polymeric microfluidic devices and their applications for electrophoretic separation. J Micromech Microeng 16(8):1681